AGU ADVANCING EARTH AND SPACE SCIENCES

Tectonics®

RESEARCH ARTICLE
10.1029/2024TC008529

Key Points:

- Using cosmogenic ^{36}Cl dating, we model the multi-millennial slip histories of three faults along strike in the Southern Italian Apennines
- The slip histories of the three faults are characterized by alternating phases of rapid slip (clusters), and quiescence (anticlusters)
- Variability in slip-rates during clusters and anticlusters can lead to significant variations in earthquake probability forecast

Supporting Information:

Supporting Information may be found in the online version of this article.

Correspondence to:

C. Sgambato,
c.sgambato@bbk.ac.uk

Citation:

Sgambato, C., Roberts, G. P., Iezzi, F., Faure Walker, J. P., Beck, J., Mildon, Z. K., et al. (2025). Millennial slip-rates variability of along-strike active faults in the Italian Southern Apennines revealed by cosmogenic ^{36}Cl dating of fault scarps. *Tectonics*, *44*, e2024TC008529. https://doi.org/10.1029/2024TC008529

Received 9 AUG 2024
Accepted 16 FEB 2025

Author Contributions:

Conceptualization: Claudia Sgambato, Gerald P. Roberts, Francesco Iezzi, Joanna P. Faure Walker, Joakim Beck
Data curation: Claudia Sgambato, Delia M. Gheorghiu, Richard P. Shanks
Formal analysis: Claudia Sgambato, Gerald P. Roberts, Delia M. Gheorghiu, Richard P. Shanks
Funding acquisition: Claudia Sgambato, Gerald P. Roberts, Francesco Iezzi, Joanna P. Faure Walker, Joakim Beck, Zoë K. Mildon
Investigation: Claudia Sgambato, Gerald P. Roberts, Francesco Iezzi, Zoë K. Mildon, Alessandro M. Michetti, Eutizio Vittori

Millennial Slip-Rates Variability of Along-Strike Active Faults in the Italian Southern Apennines Revealed by Cosmogenic ^{36}Cl Dating of Fault Scarps

Claudia Sgambato[1], Gerald P. Roberts[1], Francesco Iezzi[2], Joanna P. Faure Walker[3], Joakim Beck[4], Zoë K. Mildon[5], Alessandro M. Michetti[6,7], Eutizio Vittori[8], Jennifer Robertson[1], Delia M. Gheorghiu[9], and Richard P. Shanks[9]

[1]School of Natural Sciences, Birkbeck, University of London, London, UK, [2]Department of Earth Sciences, Environment and Resources, University of Naples Federico II, Naples, Italy, [3]Institute for Risk and Disaster Reduction, University College London, London, UK, [4]Center for Integrative Petroleum Research, College of Petroleum Engineering and Geosciences, King Fahd University of Petroleum and Minerals, Dhahran, Kingdom of Saudi Arabia, [5]School of Geography, Earth and Environmental Sciences, University of Plymouth, Plymouth, UK, [6]Università degli Studi dell'Insubria, Como, Italy, [7]INGV Osservatorio Vesuviano, Naples, Italy, [8]National Research Council, Institute for Geosciences and Georesources, Florence, Italy, [9]Scottish Universities Environmental Research Centre, East Kilbride, UK

Abstract We present slip versus time histories derived from in situ ^{36}Cl cosmogenic dating for three active normal faults in the southern Apennines, Italy. In this region the total extensional strain is accommodated by either a small number of faults located across strike from each other or, in places, a single fault where no other active faults exist across strike. We investigate how strain-rates on individual faults vary through time in the context of the overall geometry of the fault system. The ^{36}Cl results confirm that the San Gregorio Magno, Auletta, and Vallo di Diano faults were active in the Holocene, with each fault exhibiting alternating periods of relatively rapid and slow, or even absence of, slip. During periods of rapid slip, lasting a few millennia, the faults accumulate up to ∼5 m of slip, which we interpret as earthquake clusters. At other times, the faults exhibit no slip for time periods lasting multiple millennia. The fluctuations in slip-rates reveal the migration of activity between faults and out-of-phase behavior. Such fluctuations have important consequences for tectonic evolution and crustal rheology, and in particular for hazard estimation because they introduce considerable variability and hence uncertainty in earthquake probability calculations.

1. Introduction

Quantifying the palaeoseismic history of faults is essential for seismic hazard analyses and can provide information on the physical mechanism responsible for fault interactions over multiple earthquake cycles (Cowie et al., 2017; Mildon et al., 2022). Some insights into the activity of faults can be inferred through historical records and palaeoseismological analyses. However, historical records only date back a few centuries, or a thousand years at best (e.g., the catalog of strong earthquakes in Italy and Mediterranean area; Guidoboni et al., 2018, 2019). Traditional palaeoseismic trenching can extend the record of slip back thousands of years (Galli et al., 2006; Pantosti, Schwartz, & Valensise, 1993), a time period that may not contain enough information to fully characterize the long-term slip-rate that include numerous seismic cycles. This is of particular concern because earthquake activity is known to cluster in time, in that multiple surface faulting earthquakes have been documented to occur in bursts over relatively short periods of time, followed by periods of low or no activity (Beck et al., 2018; Benedetti et al., 2013; Dolan et al., 2007, 2016, 2024; Iezzi et al., 2021; Kagan & Jackson, 1991; Mechernich et al., 2018; Mildon et al., 2022; Sieh et al., 1989). Previous studies that document this behavior for normal fault systems have been focused on fault systems with relatively complex geometries that include multiple parallel faults across strike, where the slip activity can switch across strike between faults, in order to maintain the regional strain-rate (Cowie et al., 2017; Iezzi et al., 2021; Mildon et al., 2022; Nicol et al., 2006). The question arises as to how faults systems that are more localized, with few faults across strike, behave over multiple millennia. Over a shorter timescale (tens to hundreds of years) it has been shown that the orientation, number, and geometry of faults determine a geometry-specific behavior in the stress evolution associated with earthquake recurrence, such that the complexity of a fault system geometry may control how earthquakes are distributed in space and time (Sgambato, Faure Walker, et al., 2020; Sgambato et al., 2023). Examples are needed to investigate the long-term interaction occurring among faults that are located along strike. We study the Southern Apennines, Italy, because this area is characterized by a

Methodology: Claudia Sgambato, Gerald P. Roberts, Francesco Iezzi, Joakim Beck, Delia M. Gheorghiu, Richard P. Shanks
Resources: Gerald P. Roberts, Francesco Iezzi, Alessandro M. Michetti, Eutizio Vittori, Jennifer Robertson
Software: Joakim Beck
Supervision: Gerald P. Roberts, Joanna P. Faure Walker
Validation: Joanna P. Faure Walker, Joakim Beck
Visualization: Claudia Sgambato, Alessandro M. Michetti, Eutizio Vittori, Jennifer Robertson
Writing – original draft: Claudia Sgambato
Writing – review & editing: Claudia Sgambato, Gerald P. Roberts, Francesco Iezzi, Joanna P. Faure Walker, Joakim Beck, Zoë K. Mildon, Alessandro M. Michetti, Eutizio Vittori, Jennifer Robertson

simple geometry, with either a small number of faults across strike or a single fault accommodating all the across-strike strain (Figure 1). Available data on fault activity rates in the Southern Apennines are mainly based on palaeoseismological analyses, covering a time period of several millennia, plus decadal geodetic results (D'Addezio et al., 1991; Devoti et al., 2014; Galli et al., 2006; Pantosti, Schwartz, & Valensise, 1993; Serpelloni et al., 2005, 2022). However, palaeoseismology shows that average earthquake recurrence intervals are on the order of hundreds to thousands of years (e.g., Caggiano fault: 1,600 years (Galli et al., 2006); Irpinia fault: 300 years (Galli & Peronace, 2014); 1,684–3,140 years (Pantosti, Schwartz, & Valensise, 1993); Val d'Agri fault: 2,500 years (Benedetti et al., 1998); Northern Matese fault: 1,700 years (Galli & Galadini, 2003)), and only a few millennia are covered by the data, so knowledge of activity rates over multiple seismic cycles is limited. The ^{36}Cl cosmogenic dating approach allows recovery of longer slip histories from normal faults, providing information on slip-rate changes over multi-millennial timescales (Beck et al., 2018; Benedetti et al., 2003, 2013; Cowie et al., 2017; Goodall et al., 2021; Iezzi et al., 2021; Mildon et al., 2022; Mozafari et al., 2019, 2021; Palumbo et al., 2004; Schlagenhauf et al., 2010, 2011).

Using ^{36}Cl cosmogenic dating of tectonically exhumed fault scarps, we investigate the multi-millennial slip history of three normal faults located approximately along strike in the Italian Southern Apennines: the San Gregorio Magno, Auletta and Vallo di Diano faults (Figure 1). The results highlight episodic behavior on these faults, with alternating earthquake clusters and periods of quiescence. The faults are ∼35 km long, but periods of rapid slip lasting a few millennia exhibit slip of up to 4–5 m, implying temporal clusters of surface faulting earthquakes. Moreover, we recognize an out-of-phase activity on the Auletta and Vallo di Diano faults, and we interpret this behavior as possibly being driven by their geometry and orientation. The results presented are the first data on the multi-millennial seismic history of active faults in the Southern Apennines, one of the regions of highest seismic hazard in Italy, and provide insights into our understanding of fault interaction and its application to fault-based seismic hazard assessment.

2. Geological Background

The Southern Apennines are undergoing extension with direction northeast-southwest, confirmed by historical and instrumental seismicity (Rovida et al., 2020, 2022) and geodetic data (Serpelloni et al., 2005, 2022). The regional extension is accommodated since 2–3 Ma by normal faults orientated northwest-southeast (Aiello et al., 2007; Amicucci et al., 2008; Ascione et al., 2003, 2007; Cavinato & De Celles, 1999; D'Agostino et al., 2001; Giano et al., 2014; Gioia, Schiattarella, et al., 2011; Villani & Pierdominici, 2010), with lengths up to ∼35 km, characterized by low slip-rates (0.2–0.67 mm/yr; Faure Walker et al., 2012; Papanikolaou & Roberts, 2007; Sgambato, Faure Walker, et al., 2020; Sgambato et al., 2023), and capable of producing damaging earthquakes of magnitude up to Mw 7.1 (Rovida et al., 2020, 2022) (Figure 1). Some of the strongest events recorded in Italy occurred in this area, such as the 1980 Irpinia earthquake (Mw 6.8; 3,000 deaths), the first event in Italy for which surface rupture was recognized along the fault trace for a length >30 km (Pantosti & Valensise, 1990; Westaway & Jackson, 1987), and the 1857 Val d'Agri earthquake (Mw 7.1), that caused ∼10,000 deaths (Figure 1).

There is some debate about whether the sampled faults are active, based on interpretation of geomorphological features such as scarps on alluvial fans (Giano et al., 2014; Villani & Pierdominici, 2010), underlining why we decided to provide more data with our studies of ^{36}Cl. The debate about whether the faults are active or not is important because all three sampled faults are suggested to have ruptured in historical times. The San Gregorio Magno fault possibly ruptured with a Mw 6.3 earthquake in July 1561 (Sgambato, Faure Walker, et al., 2020); about a month later, a Mw 6.7 event occurred with epicenter near the Auletta fault and damage extending toward the Vallo di Diano fault (Rovida et al., 2020, 2022) (Figure 1). The complexity of the regional structures (e.g., see Chiocci et al., 2023) has led to different interpretations on the link between the short fault segment herein called Auletta fault (∼3 km) and other faults in the area (e.g., Bello et al., 2022; Galli et al., 2006; Sgambato, Walker, & Roberts, 2020; see dashed line in Figure 1). The increase in post-glacial displacement toward southeast across the Auletta fault and the measured slip vector azimuth with a ∼SSW direction suggest that this fault segment is part of the Vallo Di Diano fault system, which controls a major Quaternary basin (Figure 1) (Faure Walker et al., 2012; Papanikolaou & Roberts, 2007; Sgambato, Walker, & Roberts, 2020). The combined length of the two fault segments would suggest a total length of ∼35 km. Other interpretations based on macroseismic observations of the 1561 and 1857 earthquakes, and palaeoseismological analyses, link the Auletta segment to the Caggiano fault (Figure 1) (Galli et al., 2006). Alternatively, the Auletta fault has been hypothesized to be linked to the Val d'Agri

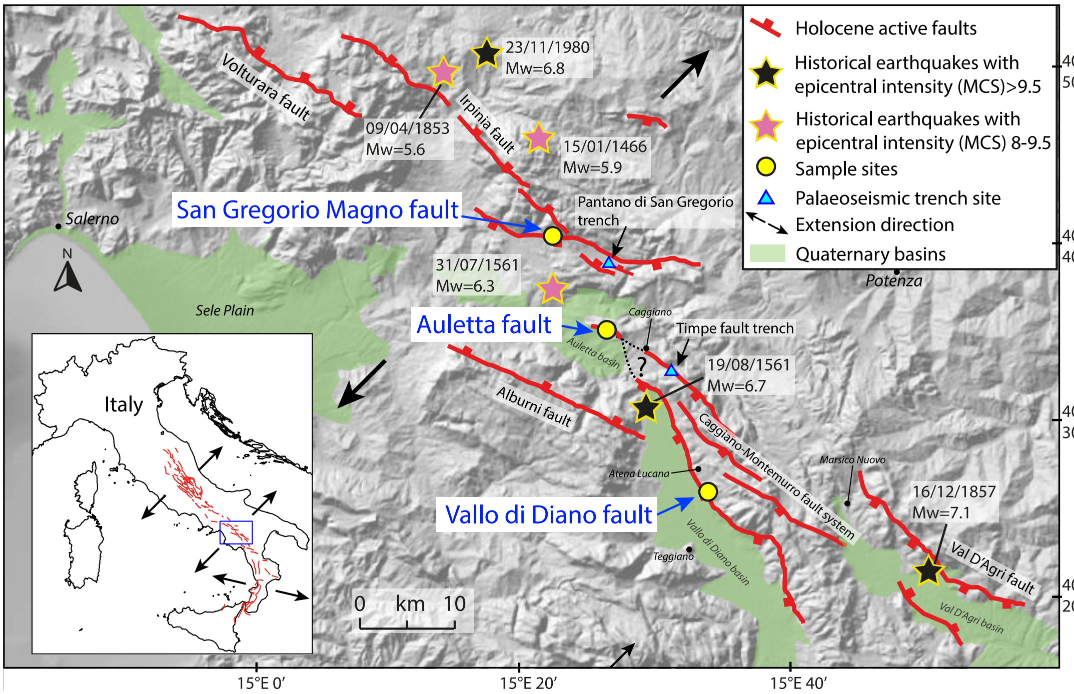

Figure 1. Location map of the study area and ^{36}Cl sample site locations. The three sample sites, indicated with yellow dots, are located approximately at the center of each fault. Locations of palaeoseismological trench at Pantano di San Gregorio Magno (D'Addezio et al., 1991) and at Timpe di Caggiano (Galli et al., 2006) are indicated with blue triangles. Dashed black line shows debated link between Auletta and Vallo di Diano faults and Auletta and Caggiano-Montemurro faults (see Section 2). Epicenters of strong historical earthquakes are indicated with stars. The studied faults are hypothesized to have ruptured in historical times.

fault (Bello et al., 2022) through a trans-ridge structure, called Caggiano-Montemurro fault (Figure 1), consisting of multiple segments, including the Caggiano fault described by Galli et al. (2006), for a total length of ~65 km; the fault is suggested to be responsible for the 1857 earthquake (Bello et al., 2022).

Following the destructive Mw 6.8 1980 Irpinia earthquake, palaeoseismological analyses were conducted at Pantano di San Gregorio Magno, across a northeast dipping segment first recognized after the 1981 event (Bollettinari & Panizza, 1981), that is a continuation of the Irpinia fault (Figure 1). Five events were recognized in the trench at Pantano di San Gregorio, dated at 11,180–19,660 B.P., 6620–9420 B.P., 2570–6620 B.P., 1720–2570 B.P., and 1980 C.E. (D'Addezio et al., 1991), in good agreement with the earthquakes dated at a trench site on the Irpinia fault section (Pantosti, Schwartz, & Valensise, 1993). No surface rupture was recognized along the southwest dipping San Gregorio Magno fault, the subject of our work, after the 1980 earthquake (Pantosti & Valensise, 1990).

Palaeoseismological analysis along the Timpe fault, considered by some authors as the southernmost segment of the Caggiano fault (Bello et al., 2022; Cello et al., 2003; Galli et al., 2006) and considered as a possible continuation of the Auletta fault (see dashed line in Figure 1), indicated ruptures linked to five events that occurred at ~7000 B.P., 6500–4500 B.P., 4500–2500 B.P., and two events that occurred after 2500 B.P., hypothesized to have occurred during or after the fifteenth and nineteenth centuries, thus possibly coinciding with the 1561 C.E. and 1857 C.E. events (Galli et al., 2006). Based on its damage distribution, it has been hypothesized that the 19^{th} of August 1561 event possibly simultaneously ruptured the Auletta and Vallo di Diano faults (Sgambato, Faure Walker, et al., 2020). The 1857 Mw 7.1 event is believed to have ruptured the Auletta and Caggiano faults, and a few minutes later the Val d'Agri fault (Benedetti et al., 1998; Cello et al., 2003; Galli et al., 2006) (Figure 1).

3. Methods

3.1. Sample Sites Characterization

We sampled the San Gregorio Magno, Auletta and Vallo di Diano faults for ^{36}Cl, because their location and orientation allowed us to explore the multi-millennial behavior of along-strike faults. The locations of the sites are: 40.671666°–15.379235° for the San Gregorio Magno site, 40.580551°–15.454045° for the Auletta site, 40.414705°–15.573636° for the Vallo di Diano site. It has been noted that the exhumation of the Auletta (or Monte San Giacomo) fault scarp has been influenced by a combination of erosion/mass-wasting and recent tectonic motion (Ascione et al., 2007; Galli et al., 2006). Indeed, exhumation on all our sampled faults varies spatially between that produced by pure tectonic fault slip and a combination of tectonic fault slip and erosion/mass-wasting. Our fieldwork along many scarps in the Apennines shows that gully erosion is widespread, with the Auletta scarp being no exception. For example, on the Auletta scarp, gullies that are ~2–3 m in width are spaced ~3–15 m apart along strike in some sections of the fault, separated by intervening slopes that are unaffected by gully erosion (Figure S2a in Supporting Information S1). This means that, like all the fault scarps we have investigated, only a very small part of the Auletta scarp was suitable for ^{36}Cl sampling. The suitable part of the scarp was <~8 m in along strike extent, with the fault plane preservation only suitable in a 1–2 wide portion of this <~8 m site (e.g., Figure S2a in Supporting Information S1). The very small size and limited extent of sites suitable for ^{36}Cl sampling is ubiquitous in the Apennines, and this has been noted in previous publications (Cowie et al., 2017; Goodall et al., 2021; Mildon et al., 2022; Roberts et al., 2024). Thus, we emphasize that we have been very careful to choose sample sites that avoid gully erosion, ensuring that fault plane exhumation is the result of tectonic processes only, with zero or minimal erosion of the hanging wall colluvium. This approach was formalized in Cowie et al. (2017). In more detail, at each site the contact between lower slope and fault plane and upper slope and fault plane is planar and almost perfectly horizontal, indicating no erosion and/or sedimentation in the Holocene after the demise of the Last Glacial Maximum (LGM) (15 ± 3 ka); the fault plane is continuous along strike around the sample site, and gullies and alluvial fans are tens of meters distant from the sample site (Figures S1, S2 and S3 in Supporting Information S1). The planarity of the lower contact has been checked at each sample site by constructing an along-strike profile, using a 30 cm ruler (Figures S1j, S2i, and S3j in Supporting Information S1). This along-strike profile will reveal a non-planar contact between the lower slope and the fault plane if hangingwall gully erosion is present, but our sampled sites show profiles that are close to being planar with undulations generally <±30 cm in vertical dimension. Some small gullies and colluvial wedges are present elsewhere along the fault planes, in places just a few meters along strike, however the sampling sites are located on planar sections (Figure S1j, S2i, and S3j in Supporting Information S1). We emphasize that this approach to selecting a site is vital, because the ^{36}Cl data alone cannot be used to differentiate between tectonic slip and exhumation through erosion/mass-wasting without such observations. The sampled fault planes are well preserved, with millimeter-scale preserved striae, indicating minimal erosion. A ~1 m deep trench was excavated, to collect samples below the ground surface, and to constrain the subsurface ^{36}Cl production rate and infer the most recent slip history. The trench exposes the stratigraphy of the colluvium, where the contact between the darker organic-rich Holocene deposits and the underlying compacted fine grain matrix with angular limestone clasts deposited during the LGM can be recognized; this contact is used as the height of sample 0 (Figures S1–S3 in Supporting Information S1). A scarp profile has been constructed at each sample site (Figures S1i, S2h, and S3i in Supporting Information S1), to constrain important parameters used to model the slip history, such as the Holocene slip, the dip of upper slope and lower slope, and the fault dip. The profiles were constructed using chain surveying technique where the dips of 1 m sections of the slope were measured with a clinometer and plotted to construct a topographic profile. The average inclination of the upper slope and lower slope is interpreted, and the vertical offset is measured as vertical distance between the projections of the upper slope and lower slope surfaces onto the fault plane (Figures S1i, S2h, and S3i in Supporting Information S1). Samples collected have dimensions of 15 × 5 × 2 cm and are spaced ~20–30 cm. Samples have been collected up the dip of the fault plane, but where the fault plane preservation was not optimal, a better-preserved part of the fault plane has been sampled by stepping to the side (Figures S1c, S2c, and S3c in Supporting Information S1). Discontinuous sampling has been shown to provide results that are indistinguishable from more continuous sampling (Iezzi et al., 2021; Mildon et al., 2022). Studies that progressively removed up to 75% of the samples from a semi-continuous sampling and remodeled the fault slip-histories, found that spacing up to ~50–100 cm, larger than the spacing between samples in this work, are sufficient to resolve the same magnitude and timing of slip-rate variations than those modeled from the full data sets (Iezzi et al., 2021; Mildon et al., 2022). Thus, we are confident that our approach is robust. Note that a sample collected at 350 cm on the Auletta fault scarp could not be included in the analyses, as the Accelerometer Mass Spectrometer (AMS) measurement of ^{36}Cl was corrupted by a high content in Sulfur (^{36}S) in the sample, which caused interference. Thus, the spacing between the two uppermost samples of the Auletta fault is >100 cm.

3.2. Upper Slope Sample Site Characterization

We collected three samples from the upper slope of each sampled fault, a technique advocated by Dunai (2010) to constrain the ages at which the high erosion rates characterizing the LGM diminished, allowing stabilization of the slope, and thus preservation of the scarps. The choice of a sample suitable for exposure age analyses is complicated, as the site for sampling must have specific characteristics.

We assume that post-LGM erosion has affected many, but not all the available rock outcrops. Thus, we only sample where we think we have identified a bedrock surface that stabilized during the climate change during the demise of the LGM. The samples should be collected from up-standing pinnacles with rounded tops, possibly characterized by rillenkarren that indicate a long exposure (Figures S4–S6 in Supporting Information S1). Thus, we only sample pinnacles that are among the highest on the surface, and do not show a flat top or sharp surfaces that may indicate that blocks that may had previously been on the top have toppled off since the demise of the LGM (Figure S4–S6 in Supporting Information S1). We assume and hence test the hypothesis that the rounded top pinnacles are surviving remnants of the LGM surface (Figure S7 in Supporting Information S1), and that the imperfect fractured-top pinnacles developed due to erosion of formerly rounded top pinnacles. Unfortunately, the rounded-top pinnacles are relatively rare, as this is the nature of the limestone surface where the samples are collected, with most of the pinnacles on the upper slope surface having fractured tops possibly indicating topping of blocks off the top of the pinnacles after the demise of the LGM, and hence are not suitable for sampling (Figures S4–S6 in Supporting Information S1). Cover of the 30–50 cm high rounded-top pinnacle by post demise of the LGM sediments is unlikely, as (a) such sediment is rare, covering only 15%–20% of the surface area at most and (b) sediment thicknesses are only ∼10–15 cm at most (see Figures S4–S6 in Supporting Information S1). In other words, sediment flux across the upper slopes after the demise of the LGM was very low, consistent with the post-LGM erosion rates measured through denudation of the faults planes of ∼0.001 mm/yr (Tucker et al., 2011).

3.3. Samples Preparation

The sample preparation requires two main steps: (a) a reduction of the sample size by mechanical means, and (b) a chemical dissolution.

During the first phase, the samples are reduced in size and sieved to separate the 125–250 μm and <125 μm fractions. The 125–250 μm is then used for the chemistry process. The chemistry process has been carried out by SUERC, Scottish Universities Environmental Research Center. The chemical procedure, as outlined in Stone et al. (1996) and Schlagenhauf et al. (2011), is summarized as follows: each sample is leached and then dissolved with nitric acid (HNO_3); the samples are spiked with a Cl carrier to increase the concentration of chlorine, this aids the measurements of Cl concentration in the AMS; after the dissolution, the samples are decanted and then centrifuged, to remove any residual of solid sediment; silver nitrate ($AgNO_3$) is added to the solution, so that all the chlorine present in the solution will react to form silver chloride (AgCl); AgCl is precipitated out of the sample by acidification, washed, dried and finally packed into accelerator plugs. Finally, the AMS measures both ^{36}Cl and Cl_{nat}.

3.4. Modeling of ^{36}Cl Concentrations and Slip Histories

The ^{36}Cl concentrations and the displacement histories of the studied faults have been modeled using a Bayesian Reversible Jump Markov-Chain Monte Carlo (MCMC) algorithm published by Beck et al. (2018). The code searches for the highest probability for the distribution of slip histories, given the measured data, generating two parallel Markov chains of random samples from the probability distribution, where the initial sample is taken from the prior distribution, and the next sample in the chain is only dependent on the last sample that was drawn. The process is repeated multiple times, until the convergence between the distribution of the samples and the desired distribution is reached. A Gelman-Rubin (GR) test (Gelman & Rubin, 1992) ensures that the convergence between two parallel Markov chains has been reached (Beck et al., 2018), typically ∼1,000,000 runs are needed. To monitor if a chain has converged to the target distribution, it is compared to another randomly initialized chain. The GR test makes a comparison of the variance of samples within each Markov chain and the variance between Markov chains. The potential scale reduction factor (PSRF) is the ratio of the two variances (Figure 2ii), and it will approach 1 with infinite iterations. If chains are at equilibrium, the PSRF will be equal to 1; if the chains have not converged to a common distribution, the PSRF will be >1. Gelman and Rubin (1992) recommend that all the parameters in the independent Markov chains must be sampled until the values for PSRF are <1.1. In our

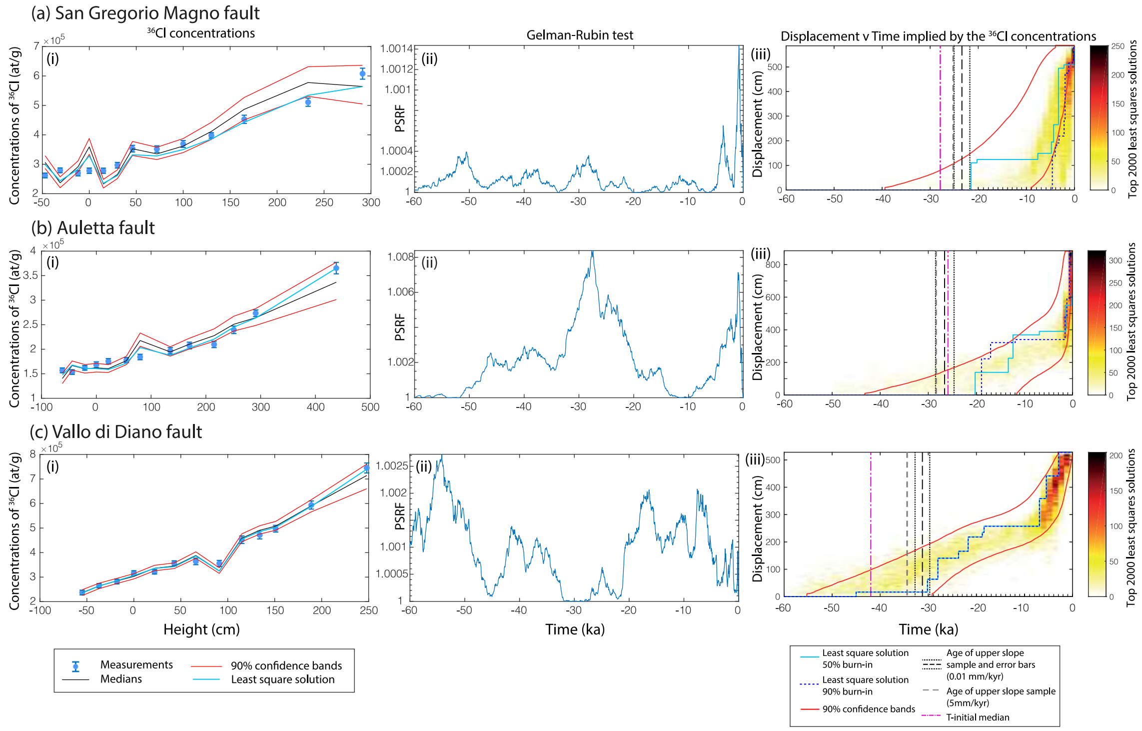

Figure 2. Modeled slip histories from ^{36}Cl concentrations measured on the San Gregorio Magno, Auletta, and Vallo di Diano faults. (ai-ci) Measured ^{36}Cl concentrations and modeled Bayesian posterior distribution. The medians (black lines), least squares solutions (light blue lines), and 90% confidence bands (red lines) are shown. (aii-cii) Convergence diagnostic of the modeled Markov chains, from Gelman-Rubin test (Gelman & Rubin, 1992). Potential scale reduction factor values below 1.01 indicate convergence. (aiii-ciii) Slip histories for the three studied faults. The top 2000 least squares solutions are shown in yellow-red color scale. Light blue line shows the least squares solution obtained with a 50% burn-in. Dashed blue line shows the least squares solution obtained with a 90% burn-in. The 90% confidence lines are in red. The age of upper slope samples and their uncertainties calculated with an erosion rate of 0.01 mm/kyr using CRONUScalc online calculator (Marrero et al., 2016) are plotted as vertical dashed black lines. The age of upper slope samples calculated with an erosion rate of 5 mm/kyr are plotted as vertical gray lines. The T_{init} median, that is, the time after which the erosion stops and the slip from earthquakes is recorded, iterated by the Markov-Chain Monte Carlo code, is plotted as vertical dashed pink line.

analyses, PSRF are <1.01 for all faults. Since MCMC algorithms are sensitive to their starting point, an initial burn-in phase should be applied, to remove initial results before the convergence of the least squares solutions. Figure 3 shows the least squares solution obtained with a burn-in of 50% and 90%, while the top 2000 least squares solutions (yellow to red rectangles) have a 50% burn-in applied. Other combinations of top 500, 2,000, and 10,000 solutions with 50% or 90% burn-in are shown in Figures S9–S13 in Supporting Information S1. Input data such as dip of fault scarp, dip of upper slope and lower slope, and amount of slip, are taken from direct measurements on the fault plane and interpretation of the fault scarp profile. Since it is unlikely that the slip per earthquake is constant, the value of slip per event is iterated, and the code iterates the coseismic slip in the range of 10–300 cm, with the higher value ~3 times higher than the expected slip for the average magnitude calculated for these fault lengths (~35 km) (calculated from Wells and Coppersmith (1994) relationship).

The code models the slip histories in a time window that can be set by the user. Specifically, the values assigned for T_{min} and T_{init}, as defined in Beck et al. (2018), were set at $T_{min} = 120{,}000$ years and $T_{init} = 80{,}000$ years. All other priors and settings are the same as that shown in the published code. Setting an older age of 80 ka allows iteration of the age of the initial production of ^{36}Cl before the expected age of demise of the LGM (15 ± 3 ka). The code also explores earthquake slip prior to the LGM (or a time chosen by setting the age of the initial production of ^{36}Cl before the expected 15 ± 3 ka), by picking slip events from a Brownian passage time (BPT) earthquake model, thus avoiding arbitrary interpretation for early ^{36}Cl production. We allowed the code to explore slip recorded before the LGM because results from the slip histories of some faults in Attica, Greece, showed slip as old as 50 ka (see Figure 3 in Iezzi et al., 2021).

The sampled fault scarps are smaller than the total displacement measured across the fault scarps (see scarp profiles, Figures S1i, S2h, and S3i). This is because the upper part of the fault scarps is often degraded, thus it is

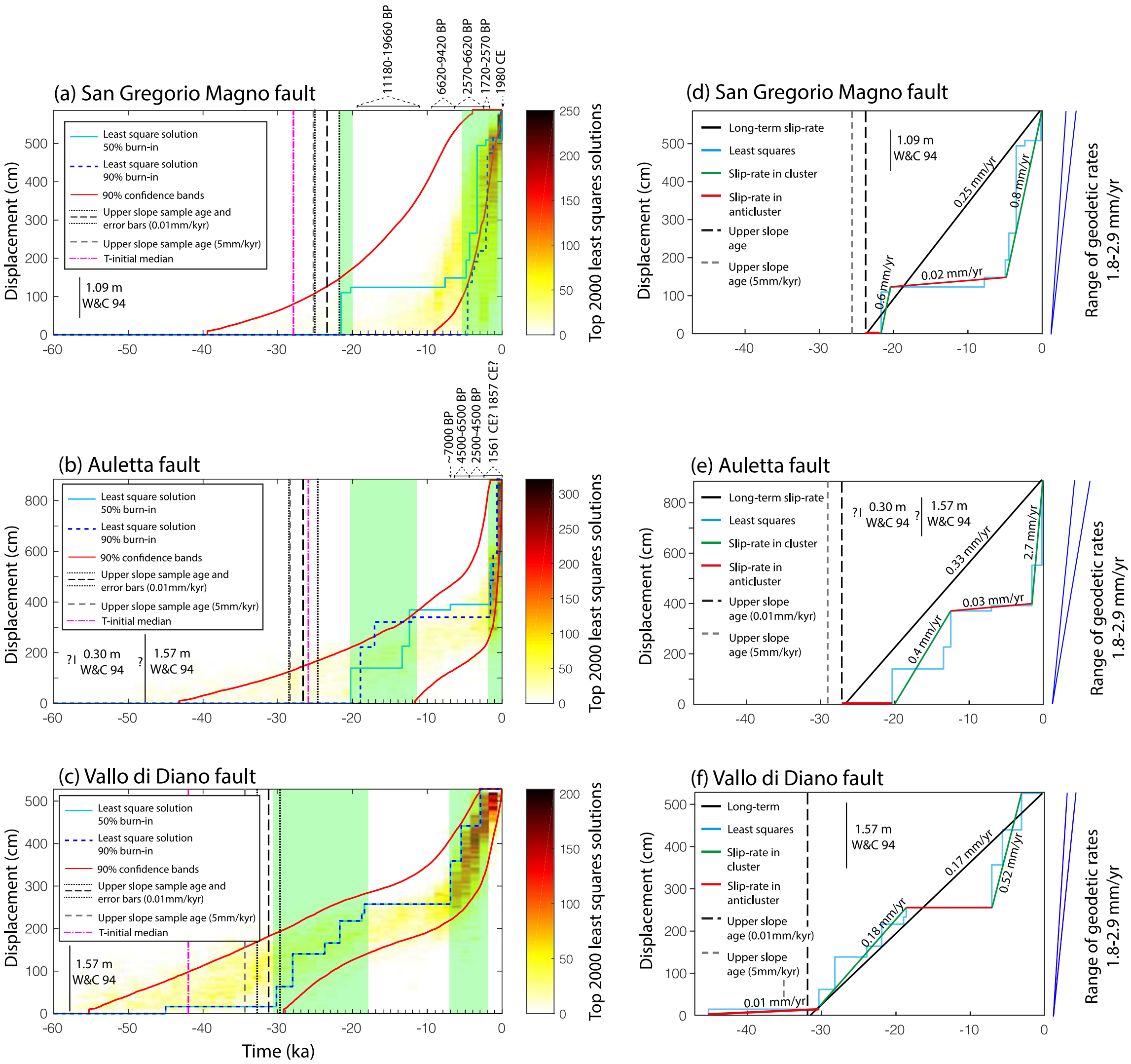

Figure 3. Interpretation of periods of rapid slip on the San Gregorio Magno (a), Auletta (b), and Vallo di Diano (c) faults inferred from modeled ^{36}Cl data. The slip histories are shown using the least squares solution obtained with a 50% burn-in (solid blue line), the least squares solution obtained with a 90% burn-in (dashed blue line), the top 2,000 least squares solutions (yellow to red rectangles), and the 90% confidence intervals (red line). Our interpretations of the timing of periods of high slip-rate are shown as green rectangle. Black arrows indicate radiocarbon ages from a palaeoseismological trench at Pantano di San Gregorio Magno (D'Addezio et al., 1991), near the San Gregorio Magno fault, and a trench at Timpe di Caggiano, near the Auletta fault (Galli et al., 2006). The timing of palaeoearthquakes broadly agree with the slip history inferred from ^{36}Cl data of the San Gregorio Magno fault, whereas only the two most recent trench events coincide with the slip at 2 ka to present for the Auletta fault. (d)–(f) Interpretation of the slip-rates during clusters and anticlusters. Displacement during periods of high slip-rates is larger than expected values of the maximum slip in a single earthquake calculated from Wells and Coppersmith (1994) length-displacement relationship, suggesting these time periods contain temporal clusters of several surface faulting earthquakes. For the Auletta fault, the shown displacement refers to either the length of individual fault segment (7 km, maximum displacement 0.30 m) or total length when linked to the Vallo di Diano fault (~35 km, maximum displacement 1.57 m). The insets to the right of (d), (e) and (f) with blue lines show summed slip-rates across the entire Apennines in the studied region implied by geodetic data, scaled so that the slopes of blue lines can be compared with rates implied by the ^{36}Cl data.

not possible to sample the entire fault scarp as this is not entirely preserved. However, we can gain information about the history of exhumation of the now eroded upper parts of the fault because samples taken from the preserved part of the fault planes contain information about the exposure of the now eroded higher parts of the fault plane. This is because the preserved fault plane samples were accumulating ^{36}Cl at depth beneath the now eroded samples. The code includes calculations of ^{36}Cl accumulation before the demise of LGM, stretching as far back to 80 ka, when samples were in the subsurface, performing millions of iterations of ^{36}Cl production with varying spallogenic and muonic production rates, spallogenic and muonic attenuation lengths, and colluvial densities, with exhumation iterated millions of times by drawing from a BPT model of earthquake slip amounts and timings, explicitly including the possibility of slip-rate variability and temporal earthquake clustering.

Included in the modeling are information on ^{36}Cl concentrations and their uncertainties, concentration of Cl_{nat}, and concentration of the main elements, expressed as oxides, such as SiO_2, Al_2O_3, Fe_2O_3, MnO, MgO, CaO, Na_2O, K_2O, TiO_2, P_2O_5, elements in traces, both in the bedrock samples and in typical Apennines colluvium that reflects weathered carbonate and volcanic ash material; we also include and height and thickness of the samples for the fault plane samples (Table S5 in Supporting Information S2). Information on the chemical composition of the colluvium is derived from a sample collected in central Italy, whose characteristics are comparable to those of the Southern Apennines (Table S4 in Supporting Information S2). Scaling factors have been used to calibrate the ^{36}Cl production due to spallation and neutron and muon capture variations due to latitude and elevation changes, following Stone (2000) (Table S3 in Supporting Information S2). However, colluvium density, time of demise of LGM, spallogenic production rate, spallogenic attenuation length, muonic production rate and muonic attenuation length are iterated by the code (Figure S8 in Supporting Information S1). In our models, the medians of the priors fit within the range of values expected for production rates, attenuation lengths, colluvial densities, slip per event, scarp ages, that include 3% implied model errors (Figure S8 in Supporting Information S1).

Exposure ages of the upper slope samples were obtained using the CRONUS online calculator (Marrero et al., 2016). The calculator provides surface exposure age using data from the AMS as input, including concentration of ^{36}Cl and its uncertainty, elemental composition, elevation, shielding and erosion rates. We have iterated the erosion rates that we input in the CRONUS code from 0.01 to 5 mm/kyr, with the highest value similar to those applied in previous works (e.g., Mechernich et al., 2018; Stone, 2000). Long-term erosion rates calculated in the Southern Apennines have values of ~0.2–0.3 mm/yr (Amato et al., 2003; Schiattarella et al., 2008), however, these values are averaged across large areas that includes valleys and interfluves and are calculated over 0.8–0.6 Ma, a time that encompasses numerous glacial and interglacial periods. Tucker et al. (2011) calculated the Holocene erosion rate on the Magnola fault scarp in central Italy, whose exposure history has been dated with ^{36}Cl analyses by Schlagenhauf et al. (2011), and found that the rate of erosion in the Holocene was tens of times lower than the calculated late Pleistocene rate of 0.2–0.4 mm/yr. As we believe that the samples that we collect from the upper slope are remnants of the LGM surface (see Figure S7 in Supporting Information S1), they would have undergone minimal erosion. Therefore, the upper value of erosion rate is likely an overestimation. Input data and results of the CRONUS modeling are in Tables S3 and S4 in Supporting Information S2 respectively.

3.5. Earthquake Annual Rates and Probability

We used the FiSH software (Pace et al., 2016) to calculate the annual rates and probability of occurrence of earthquakes for the three studied faults, using slip-rates calculated in periods of clusters and anticlusters. The FiSH code (Pace et al., 2016) allows the calculation of expected earthquake rates from fault data, assuming that geometry and kinematics of faults are an expression of their seismogenic potential. The fault geometric parameters and slip-rates used are summarized in Table S10 in Supporting Information S2.

We used the MB (moment budget) tool (Pace et al., 2016) to calculate the seismic moment rate that is permitted by the fault, based on the Wells and Coppersmith (1994) length-magnitude scaling relationship. For each fault, we calculated the earthquake annual rates using the fault geometrical characteristics (length, dip, seismogenic thickness), the slip-rate, and the magnitude and date of the last observed earthquake from historical and palaeoseismological data. Besides the moment rates, the MB tool provides values for the maximum expected magnitude and its standard deviation, the coefficient of variation, the elapse time since the last earthquake, and the average recurrence interval. These parameters were calculated with the MB tool for different values of slip-rate, using the average slip-rate measured over 15 ka, and the slip-rate measured over periods of clusters and periods of anticlusters (Table S10 in Supporting Information S2).

The results obtained with the MB tool were then used to calculate the annual rates and probability of occurrence of earthquakes using the AR (annual rates) tool (Pace et al., 2016) (Figure 5). The AR tool returns the cumulative annual rate of earthquakes with Mw between a chosen minimum magnitude, in this case Mw 5.5, and the maximum expected magnitude, based on the Wells and Coppersmith (1994) length-magnitude relationship (Figures 5f–5h, Figures S15f–S15h, S16f–S15h, and S17f–S17h in Supporting Information S1). We calculated the annual rates of earthquakes using a truncated Gutenberg-Richter distribution (Figures 5f–5h, Figures S15f–S15h, S16f–S16h, and S17f–S17h in Supporting Information S1). The earthquake probabilities are calculated using different earthquake recurrence models: the time-dependent BPT model, the time-independent Poisson model, and the conditional probability of occurrence (P_{elap}) of an event given the elapsed time since the last event (T_{elap}) (Figures 5i–5k, Figures S15i–S15k, S16i–S16k, and S17i–S17k in Supporting Information S1). The BPT and P_{elap} models have been calculated for the next 50 years, and the Poisson probability is calculated over a 50-year period.

4. Results

4.1. Modeling ^{36}Cl Concentrations

Concentrations of ^{36}Cl increase with height in the dip direction of the fault plane (Figures 2ai, 2bi, 2ci), following a typical profile observed in active normal faults, where the fault scarp is progressively exhumed by earthquakes and is exposed to increasing cosmic radiation (Beck et al., 2018; Benedetti et al., 2002, 2003; Cowie et al., 2017; Iezzi et al., 2021; Mildon et al., 2022; Palumbo et al., 2004; Schlagenhauf et al., 2011; Tesson & Benedetti, 2019; Tikhomirov et al., 2019). The modeled ^{36}Cl concentration profiles and the derived slip histories for the three faults are shown in Figure 2. The iterations were interrupted when the Gelman-Rubin diagnostic confirmed the convergence of the MCMC solutions for two parallel Markov chains for each of the faults (i.e., when values of potential scale reduction factor, PSRF, were <1.01; Figures 2aii, 2bii, and 2cii). We performed 1,440,862 iterations (single Markov chain iterations) for the San Gregorio Magno fault, 1,276,928 iterations for the Auletta fault, and 1,376,002 iterations for the Vallo di Diano fault. Some ^{36}Cl concentrations fall outside of the modeled 90% confidence bands, but these anomalies are considered by the MCMC code (Beck et al., 2018).

4.2. Slip-Rate Histories

The modeled slip histories are inferred for each fault by interpreting the significance of (a) the least squares solution with either a 50% burn-in and 90% burn-in, (b) the distribution of the top 2,000 least squares solutions with a 50% burn-in, and (c) the full posterior Bayesian results shown in the form of 90% confidence intervals (Figures 2aiii, 2biii, and 2ciii). The choice of the optimal burn-in is discretionary. A short burn-in period will leave some unrepresentative samples in the results, while a larger burn-in can discard samples that may give a more accurate estimate of the distribution. Thus, our preference is on the application of a 50% burn-in. We have applied a larger burn-in period to check that results were not largely different from those obtained with a 50% burn-in.

Overall, the results indicate that the slip rates on all faults are not constant through time since periods of slip accumulation and periods of little or no slip can be recognized (Figure 3). The slip that accumulates during high slip-rate periods is consistently larger than the expected maximum coseismic slip for faults of such length (∼1–1.5 m, based on Wells and Coppersmith (1994) length-displacement relationship, see Figures 3d–3f) and the total slip observed during these periods is up to ∼5 m. Thus, the periods of rapid slip must represent multiple surface faulting earthquakes, that is, earthquake clusters (Figures 3d–3f). Overall, the studied faults were active at different times in the past ∼20–30 ka, and all are characterized by an alternation of temporal earthquake clusters and anticlusters of variable durations (Figures 3a and 3c). While the San Gregorio Magno fault experienced most of its slip between ∼5 ka and Present (Figure 3a), both the Auletta and Vallo di Diano faults had up to ∼50% of their slip early in their slip histories (Figures 3b and 3c). In detail, the least squares solution with 50% burn-in suggests a period of activity for the San Gregorio Magno fault at ∼22–20 ka when the fault accumulated ∼1 m of slip (Figure 3a). However, most of the slip (∼5 m) was accumulated on the San Gregorio Magno fault within the last ∼5 ka, and this is evident with both a 50% and 90% applied burn-in. For the Auletta fault, we observe slip at ∼21–11.5 ka and from ∼2 ka to Present (Figure 3b), with small variations in the amount of slip accumulated during the two clusters obtained by using either 50% or 90% burn-in. The Vallo di Diano fault has a period of rapid slip that began at ∼30 ka, lasting until ∼18 ka (Figure 3c). A second period of rapid slip is observed between ∼7 and 2 ka; no recent slip is recorded on this fault since ∼2 ka (Figure 3c). The results for the Vallo di Diano fault are unchanged using either a 50% or 90% burn-in.

4.3. Preservation of Slip

Although it is commonly accepted that the cumulative effect of earthquakes started to be preserved after the demise of the LGM (e.g. about 15 ± 3 ka) (Cowie et al., 2017; Piccardi et al., 1999; Roberts & Michetti, 2004), our results show that the slip on the three studied faults started to be recorded before this time (Figure 3). In this

Table 1
Upper Slope Exposure Ages

Sample name	Cl in sample (ppm)	Cl in sample uncertainty (ppm)	Cosmogenic atoms ^{36}Cl/gram of rock	Cosmogenic atoms ^{36}Cl/gram of rock uncertainty	CRONUScalc age (kyr)	Age uncertainty (kyr)
SG-US	18.08	0.06	871,177.38	26,556.15	23.49	1.76
AU-US	17.96	1.92	899,330.01	28,578.14	26.71	1.96
VD-US	17.55	3.89	945,267.75	40,735.30	31.32	2.49

Note. The table shows measurements of chlorine and cosmogenic ^{36}Cl, with their uncertainties, in the upper slope samples of the San Gregorio Magno fault (SG-US) Auletta fault (AU-US) and Vallo di Diano fault (VD-US), and the ages of the upper slope samples calculated in CRONUS (Marrero et al., 2016) online calculator using an erosion rate of 0.01 mm/kyr. See Table S3 in Supporting Information S2 for detail and exposure ages calculated with higher erosion rates (up to 5 mm/kyr).

section we show that these relatively old scarp ages are supported by our ^{36}Cl exposure dating that constrains the ages of the upper slopes that formed and stabilized before the formation of the preserved fault scarps.

In detail, the results from the top 2,000 least squares solutions for 50% burn-in suggest that slip was recorded on the San Gregorio Magno fault starting from ∼35–2 ka, on the Auletta fault from ∼49–15 ka, and on the Vallo di Diano fault from ∼58–25 ka (Figure 3). The range suggested by the 90% confidence intervals are ∼39–9 ka for the San Gregorio Magno fault, ∼42–12 ka for the Auletta fault, and ∼55–30 ka for the Vallo di Diano fault. The wide range of ages of preserved slip is in part due to the older slip history of the faults not being as well-constrained as its most recent part, since the top of the fault plane is eroded and hence not sampled (see upper degraded scarps in Figures S1–S3 in Supporting Information S1).

More information can be gained from the age of the samples that we collected from up-standing pinnacles on the upper slopes (Figures S1–S3 in Supporting Information S1), which indicate the age of the surface pre-faulting, after high erosion rates characterizing the LGM decreased, allowing the Holocene slip to be preserved. The ages and uncertainty of the upper slope samples, marked as dashed black lines in Figure 3, have been constrained using the CRONUS online calculator (Marrero et al., 2016). For the San Gregorio Magno fault, the upper slope age ranges between 23.49 ± 1.76 kyr and 25.26 ± 1.96 kyr; for the Auletta fault the age range is between 26.71 ± 1.96 kyr and 28.67 ± 2.3 kyr; for the Vallo di Diano fault, is 31.32 ± 2.5 kyr and 34.53 ± 2.99 kyr. These ages were calculated using erosion rates of 0.01–0.5 mm/kyr (Table 1, Tables S3 and S4 in Supporting Information S2).

In summary, it is clear that the slopes that were ultimately to be offset by the fault scarps stabilized before 15 ± 3 ka, the widely expected age for the LGM (Allen & Huntley, 2009; Giraudi & Frezzotti, 1997; Roberts & Michetti, 2004). Since the upper slope ages have been independently constrained using CRONUS calculator (Marrero et al., 2016), they act as an independent control of the ages of initial recorded slip indicated by the least squares solution inferred by the MCMC code (Beck et al., 2018).

Figure 3 also shows the median of the T_{init} from the posterior distribution of results produced by the iterations conducted (*sensu* Beck et al., 2018), with T_{init} defined as a single point in time before which all the scarp is eroded by high-rates of cold-climate erosion, and after which the erosion slows and essentially ceases, so that slip from earthquakes can be recorded. The T_{init} values and the upper slope sample ages should represent a similar point in time as they both refer to the time when periglacial slopes stabilized due to warming climate. The T_{init} median for the San Gregorio Magno fault is 28 kyr, for the Auletta fault is 25.9 kyr and for the Vallo di Diano fault is 42.4 kyr. While the T_{init} medians for the San Gregorio Magno and Auletta faults are similar to the ages of their respective upper slope samples (Figures 3a and 3b), for the Vallo di Diano fault there is a difference of ∼11 kyr (Figure 3c). However, the value for the T_{init} 95% quantile for the Vallo di Diano fault (32.3 kyr, Table S2 in Supporting Information S2) falls within the uncertainty of its upper slope age (31.3 ± 2.5 kyr). The key result is that estimations of the upper slope age from ^{36}Cl ages derived from the CRONUS calculator (Marrero et al., 2016) and calculations of T_{init} from the code from Beck et al. (2018) are in close agreement, and are consistent with the ages when preservation of slip is suggested by the least squares solutions; slip was recorded from just after the slopes appear to have been stabilized.

Overall, the results show that the recovered slip history for these faults extend further back in time than the expected post-LGM age (15 ± 3 ka). We suggest this is consistent with the difference in age of slip preservation due to latitude and elevation observed elsewhere (Attica, Greece; Iezzi et al., 2021; Crete, Greece; Mechernich et al., 2023). The age difference has been attributed to different erosion rates related to frost-shattering, which increases with elevation, thus suggesting that faults at lower elevation are less eroded and their scarps preserve a longer portion of the slip history (Iezzi et al., 2021).

5. Discussion

^{36}Cl studies have been increasingly used to derive the multi-millennial slip histories of active faults, providing evidence of the temporal variability of fault slip-rates, and hence of earthquake recurrence, and highlighting the challenges incurred by probabilistic seismic hazard assessment. Ideally, information on earthquakes over a long timescale should be derived using all possible sources, from historical seismicity, studies of palaeoseismic trenches and slip derived from ^{36}Cl analyses, but reconciling results derived from different sources can be challenging. However, our results are encouraging, since the information derived from our ^{36}Cl analyses have been confirmed by other independently constrained results.

First, the results derived from the upper slope exposure ages show that the slopes stabilized just before slip started on the faults, and hence this result is independent from, yet consistent with, the ages of initial recorded slip indicated by the least squares solution inferred by the MCMC code (Beck et al., 2018). Figure 3 shows that the first recorded slip inferred by the least squares solution sits within the uncertainties of the exposure ages of the upper slope samples, except for the Auletta fault; we discuss this in the context of the out-of-phase activity of the Auletta and Vallo di Diano faults below. Results indicating older ages of the upper slope compared to the first recorded slip from the least squares solutions are consistent with findings from analyses of fault scarps and upper slopes on some faults in Central Italy (Cowie et al., 2017), and faults in Crete (Mechernich et al., 2023). This suggests that the ages of upper slope and thus the age at which slip can be preserved, may be dependent on latitude, local climate, and elevation, as previously suggested by Iezzi et al. (2021) from observations of fault scarps located at different elevations in Attica, Greece.

Second, our results agree with those obtained from traditional palaeoseismic trenching analyses. The proximity of two trenches near the San Gregorio Magno and Auletta faults presented an opportunity to compare ages of palaeoearthquakes with results derived from ^{36}Cl analyses (see Figure 1 for location of trenches and our own sampling). Our results show that the events recognized at the Pantano di San Gregorio trench (D'Addezio et al., 1991) broadly agree with the periods of rapid slip derived from ^{36}Cl concentrations for the San Gregorio Magno fault (Figure 3a). In detail, the ages of the last three events (2570–6620 B.P., 1720–2570 B.P., and 1980 C.E.; D'Addezio et al., 1991) fall within the period of rapid slip observed between ∼5.5 ka and present, while the event dated at 6620–9420 B.P. is not clearly visible in the least squares solution (Figure 3a). However, we do not rule out the possibility of slip relating to this earthquake occurring on the San Gregorio Magno fault, as indeed some modeled solutions exist that indicate slip around this time (yellow rectangles in Figure 3a). Nevertheless, there is agreement between the period of anticluster observed between ∼20 and 5.5 kyr and the existence of only a single palaeoearthquake recognized during this time. The oldest event recognized in the trench (11,180–19,660 B.P.) is poorly constrained compared to the others (D'Addezio et al., 1991), but could possibly coincide with the period of slip that we observed at ∼22–20 ka (Figure 3a). Comparing the slip histories derived from concentrations of ^{36}Cl on a limestone fault scarp and earthquakes derived from ^{14}C dating of offset stratigraphy presents some challenges. Displacement measured for individual palaeoearthquakes can be distributed over several fault splays (Iezzi et al., 2023), thus records of some events may be lacking at some trench locations. Differences in sedimentation rates, erosional processes, variations in climate, can further complicate the identification of palaeoearthquakes in the stratigraphy (Blumetti et al., 2017). Despite all these uncertainties, our results are in agreement with those obtained from palaeoseismic trenching. To our knowledge, this is the first time these two methodologies have been compared and show consistent results.

We are aware that coseismic surface ruptures of the 1980 Irpinia earthquake were mapped along the Irpinia fault (also known as Mount Marzano fault system) and the fault splay at Pantano di San Gregorio Magno (Figure 1), and it has been suggested that this rupture pattern occurred multiple times in the past (Pantosti, Schwartz, & Valensise, 1993; Pantosti & Valensise, 1990). Our results suggest that the fault splay trenched at Pantano di San Gregorio Magno may also have ruptured over the past ∼20 kyr with the SW-dipping San Gregorio Magno fault that we investigated. Given the strong interconnectivity between the multiple fault splays of the Irpinia fault and the San Gregorio Magno basin, we do not exclude that seismic ruptures may involve different fault splays. For instance, the trench site could have ruptured in the past during earthquakes occurring on either the Irpinia fault or the SW-dipping San Gregorio Magno fault.

Our site on the Auletta fault is in proximity of the Timpe fault trench (Galli et al., 2006). Of the five events constrained at the Timpe fault trench, south-east of the Auletta fault, only the two most recent events (>2500 B.P.) coincide with a period of rapid slip occurred between ~2 ka and present, while the three older events (~7000 B.P., 6500–4500 B.P., 4500–2500 B.P.) do not coincide with the slip history constrained from ^{36}Cl concentrations (Figure 3b). This could be possibly attributed to partial ruptures occurring on the fault; thus, it might be that the fault section trenched by Galli et al. (2006) does not always rupture at the same time as the Auletta fault, but this is uncertain. Overall, we suggest that the increasing availability of ^{36}Cl results from fault planes and the existence of numerous palaeoseismological trenches around the world present the opportunity to combine these methodologies to obtain a more comprehensive view of the seismic history of faults, particularly those with a complex rupture pattern.

With regard to the regional tectonics and fault activity rates across the system of faults, we observe a non-synchronous exhumation of the Vallo di Diano and Auletta faults, since the periods of rapid exhumation on the Auletta fault at ~21–11 ka and ~2 ka-Present occurred during phases of quiescence of the Vallo di Diano fault (Figures 3b and 3c). This non-synchronous exhumation rules out a regional increase in erosion rates as an explanation for scarp formation, for example, the action of a pluvial period like that documented in the Alps at 4.2 ka (e.g., Zerathe et al., 2014). This is consistent with our interpretation of exhumation as due to non-synchronous phases of slip on neighboring faults. As mentioned in Section 2, there is some debate on the possible configuration and linkage of the faults in this area, where some authors consider the Auletta fault as the north-western tip of the Vallo di Diano fault (Faure Walker et al., 2012; Papanikolaou & Roberts, 2007; Sgambato, Walker, & Roberts, 2020), and others link the Auletta fault segment to the Caggiano fault (Galli et al., 2006), or suggest that it possibly links to the Val D'Agri fault, for a total length of ~65 km, the so-called Caggiano-Montemurro fault (Bello et al., 2022) (see dashed black lines in Figure 1). It is unclear which interpretation is correct, but our results from ^{36}Cl data help to further the discussion. For the latter configuration, the Vallo di Diano fault and the Auletta fault, connected to the Caggiano-Montemurro fault, would be across strike from each other, and the stress transferred from one fault would consequently reduce the differential stress on the shear-zone of the other fault, possibly inducing an anticluster, in the manner advocated for other faults located across strike elsewhere in Italy by Mildon et al. (2022). Another possibility is that the Auletta and Vallo di Diano faults are segments of the same fault (Faure Walker et al., 2012; Papanikolaou & Roberts, 2007; Sgambato, Walker, & Roberts, 2020), and thus connected at depth, but do not rupture at the same time. This is plausible because small-scale relay zones can represent barriers to rupture propagation (Stein et al., 1997), even though there are examples of seismic ruptures propagating between different fault segments (e.g., Landers earthquake; King et al., 1994). The absence of evidence of surface rupture and Holocene offsets in the area between the two fault segments (dashed line in Figure 1) could be due to a relay-zone or other barrier, so this may support the notion of slip occurring asynchronously on the Auletta and Vallo di Diano fault. This could be linked to the relatively weak interaction of the two fault segments, due to the rather large gap between the known fault traces (>~5 km both along and across strike with no along strike overlap), which would perhaps impede the rupture of the linkage zone during an earthquake (Soliva et al., 2008). This might result in the preservation at the surface, over long timescales, of the observed segmented geometry. Further evidence for the asynchronicity of the Auletta and Vallo di Diano faults may be suggested by the ~6 kyr difference observed between the age of the upper slope sample of the Auletta fault and the age of its first recorded slip inferred by the least squares solution (Figure 3b). We suggest that this gap in time between upper slope age and recorded slip for the Auletta fault could be representative of a time when the fault was in an anticluster, thus no slip was recorded at the time of stabilization of the slope. This would be consistent with the hypothesized out-of-phase activity of the Auletta and Vallo di Diano faults, since at the time indicated by the Auletta fault upper slope sample (~27 ka) the Vallo di Diano fault was in a cluster (from ~31–18 ka).

The observed variability in fault activity within the Southern Apennines system has implications for fault interaction, mechanics of continental deformation, and seismic hazard, as discussed below.

Table 2
Values of Slip-Rate Calculated Over Periods of Clusters and Anticlusters and Slip-Rate Enhancement Factor

Fault	Slip (m)	Upper slope age (kyr)	Average slip-rate (mm/yr)	Date of *cluster*/ anticluster (ka)	Duration of the *cluster*/ anticluster (kyr)	Slip in the *cluster*/ anticluster (m)	Slip-rate in the *cluster*/ anticluster (mm/yr)	Slip-rate enhancement factor
San Gregorio Magno	5.86	23.50	0.25	*22–20*	*2*	*1.2*	*0.6*	2.40
				20–5.5	14.5	0.28	0.02	
				5.5-present	*5.5*	*4.4*	*0.8*	3.20
Auletta	8.85	26.7	0.33	*20–11.5*	*8.5*	*3.4*	*0.4*	1.20
				11.5–2	9.5	0.3	0.03	
				2-present	*2*	*5.4*	*2.7*	8.14
Vallo di Diano	5.28	31.3	0.17	45–30	15	0.15	0.01	
				31–18	*13*	*2.4*	*0.18*	1.09
				18–7	0	0	0	
				7–2	*5*	*2.6*	*0.52*	3.08

Our results show that during the periods of activity, the slip on each fault is accumulated during clusters of variable duration (1–13 kyr) (Figure 3). This clustered activity suggests that these faults contribute to accommodating the regional extension at different times and to a different extent. An indication of how the slip-rate varies during clusters is given by the slip-rate enhancement factor (SRE), that is the ratio between the short-term slip-rate measured during clusters and the average long-term slip-rate (Mildon et al., 2022). Since our results show that the age of preservation of the scarp is older than 15 ± 3 kyr (Figure 3), we calculate long-term slip-rates using our measured ages for the upper slopes. The long-term slip-rates are 0.23–0.27 mm/yr for the San Gregorio fault (5.86 m slip over 23.5 ± 1.76 kyr), 0.31–0.36 mm/yr for the Auletta fault (8.85 m slip over 26.7 ± 1.96 kyr), and 0.15–0.18 mm/yr for the Vallo di Diano fault (5.28 m slip over 31.3 ± 2.5 kyr) (Table 2). Consequently, the values of SRE for the San Gregorio Magno fault are 2.40 and 3.20 for the two clusters that occur between 22 and 20 ka and 5.5 ka-present (Table 2). For the Auletta fault, the SRE is 1.20 for the 20–11.5 ka cluster, and 8.14 for the cluster occurring between 2 ka and present (Table 2). The slip-rate during the cluster occurring between 31 and 18 ka on the Vallo di Diano fault gives a SRE of 1.09, while it is 3.08 for the cluster occurring between 7 and 2 ka (Table 2). These values are comparable to those obtained for faults in the Central Apennines, where SRE values range between <1 and >4 (Mildon et al., 2022). This implies that the contribution of individual faults to accommodating the regional extension varies through time. Considering that the values for the decadal GPS extension rates measured across the Southern Apennines area range between 1.8 mm/yr (Serpelloni et al., 2005) and 2.9 mm/yr (Devoti et al., 2014; Serpelloni et al., 2022), our results show that the slip on a single fault during a cluster can be sufficient to accommodate all the regional extension. For example, the slip-rate on the Auletta fault between 2 ka and present is 2.7 mm/yr, with heave-rate 2.37 mm/yr (Table S9 in Supporting Information S2). These values of slip-rate are high when considering the length of the individual Auletta segment but would be appropriate if this fault is considered as part of a longer fault (e.g., the Vallo di Diano fault, for a total length of ~35 km, Figure 1). This implies that extensional strain is not uniformly distributed across the region, but instead is focused along specific faults during certain periods of time.

Furthermore, we observe changes in the geometry of the fault interaction through time. Figure 4 shows the evolution of fault activity in the area based on the ^{36}Cl results, highlighting that faults in this area are not all active at the same time. Instead, the activity switches back and forth, with periods of time where two of the studied faults are active at the same time (Figures 4a, 4b, 4f, and 4g), and others where none of the studied faults was active (Figure 4d). Nonetheless, if we assume that the regional extension rates are constant, one or more of the other faults in the area needed to be active at this time, and these could be the Val d'Agri and Alburni faults (7–12 ka,

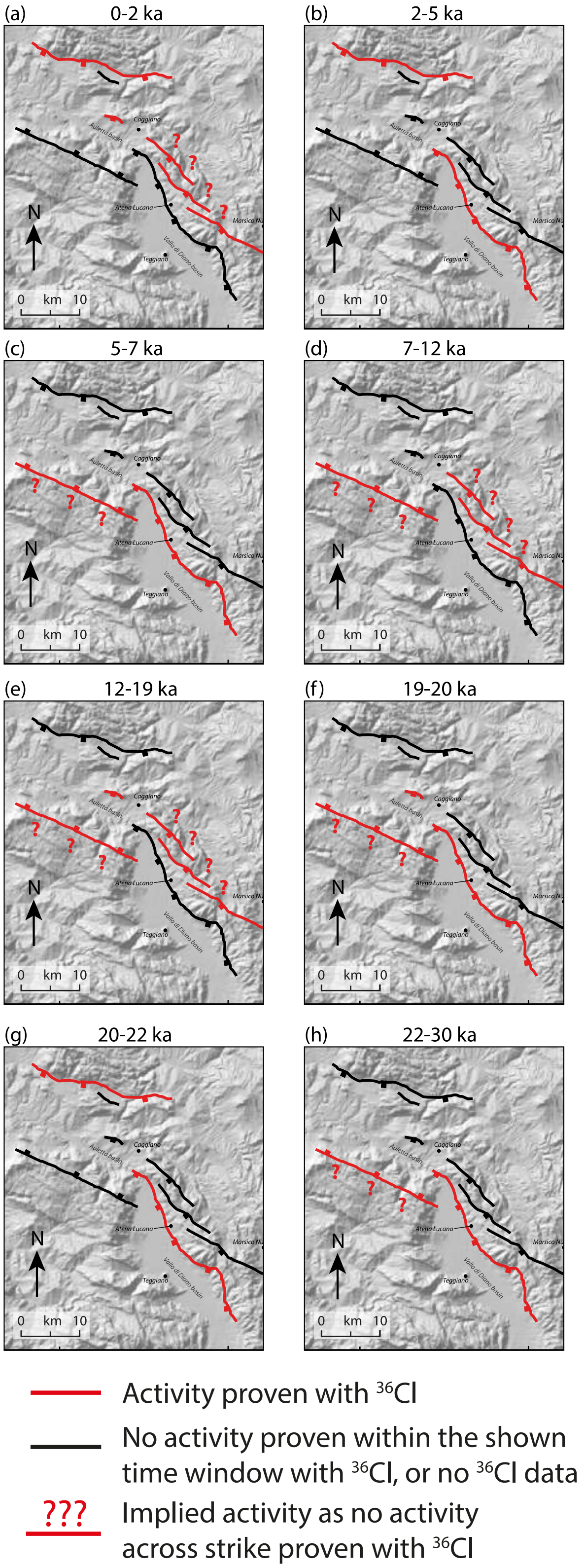
(a) 0-2 ka
(b) 2-5 ka
(c) 5-7 ka
(d) 7-12 ka
(e) 12-19 ka
(f) 19-20 ka
(g) 20-22 ka
(h) 22-30 ka
N
0 km 10
Activity proven with 36Cl
No activity proven within the shown time window with 36Cl, or no 36Cl data
??? Implied activity as no activity across strike proven with 36Cl

Figure 4.

Figure 4d). The Val d'Agri fault is considered to be responsible for the 1857 Mw 7.1 earthquake (Bello et al., 2022; Benedetti et al., 1998; Cello et al., 2003). There is no evidence of recent activity on the Alburni fault; the fault is considered to have been active between late Pliocene and late Pleistocene (Gioia, Schiattarella, et al., 2011; Soliva et al., 2008). These results imply that the geometry of the fault interaction within this fault system is changing through time, where faults that are active at the same time are sometimes en-echelon (2–5 ka, Figure 4b; 19–20 ka, Figure 4f; 20–22 ka, Figure 4g), and sometimes they dip in different directions (7–12 ka, Figure 4d; 22–30 ka, Figure 4h).

These findings indicate that slip-rates, and thus strain-rates, are variable through time, suggesting that assumption that geodetic rates can be extrapolated to longer time periods to constrain seismic hazard and continental mechanics, for example, crustal viscosity (Moore & Parsons, 2015), should be treated with caution. In terms of seismic hazard, there are considerable differences in the implied earthquake annual rates and probability of earthquake recurrence when these are calculated using average values of slip-rates calculated over the long-term, or slip-rates calculated during clusters or anticlusters (Figure 5). For example, for the San Gregorio Magno fault, slip-rate changes between 0.60 mm/yr and 0.80 mm/yr in the two clusters occurring between ∼21 and 20 ka and ∼5 ka-present, respectively (Figures 5c and 5e), while the slip rate is <0.02 mm/yr between ∼20 and 5 ka, during a period of anticluster (Figure 5d). These fluctuations lead to order of magnitude differences in the annual cumulative magnitude-frequency distributions when using the slip-rates during a cluster and an anticluster (Figures 5f–5h; Table S11 in Supporting Information S2), and therefore in the calculated probability of occurrence in the next 50 years (Figures 5i–5k; Tables S11 and S12 in Supporting Information S2), highlighting the importance of including temporal variations of slip-rates in hazard estimation.

Overall, our results emphasize that fluctuations in slip-rate, migration of activity between faults and out-of-phase behavior are an emerging theme for fault activity on millennial timescales (Dolan et al., 2016, 2024; Mildon et al., 2022). Such behavior has important implications for understanding continental mechanics and seismic hazard and warrants further study.

6. Conclusions

The earthquake histories of three faults in the Southern Apennines have been modeled from cosmogenic ^{36}Cl concentrations, to obtain information on the Holocene slip rate variations and investigate fault interaction in the region. The main findings can be summarized as follow. (a) The three studied faults show different ages for the start of slip activity, but all have been active in the Holocene. (b) The slip histories of the San Gregorio Magno, Auletta and Vallo di Diano faults are characterized by alternating phases of rapid slip (clusters) and quiescence (anticlusters) of variable duration. (c) The Auletta and Vallo di Diano faults show out-of-phase activity, so that when one fault experiences an earthquake cluster, the other is in a state of quiescence. (d) The preservation age of the bedrock fault scarps may be linked to the elevation, latitude, and climate at which the fault scarp is found, and to the age at which the fault scarp started to record slip. (e) Overall, the upper slope ages, representing a time of slope stabilization after the demise of the LGM, are comparable to the starting time of the modeled slip history; when these ages are not coinciding, it could be representative of a time in which the fault was in an anticluster. (f) Temporal variability in slip-rates has important implications for PSHA, since differences in slip-rates during clusters and anticlusters can lead to significant variations in earthquake probability forecast.

Figure 4. Fault activity through time. Red lines show faults that are active based on ^{36}Cl results. Black lines indicate faults that are not active. Fault activity switches back and forth in the system, with periods when one (c, e, h) or two (a, b, f, g) of the studied faults are active at the same time, and periods when none of the studied faults is active (d). Red lines with question marks indicate faults that, although not yet investigated with ^{36}Cl, should be active if it is assumed that regional extension rates sub-perpendicular to the fault map traces are constant through time. The Val d'Agri fault is thought to have ruptured during the Mw 7.1 1857 earthquake (Bello et al., 2022; Benedetti et al., 1998; Cello et al., 2003), whereas, although considered to have been active during late Pliocene and late Pleistocene (Brozzetti, 2011; Gioia, Schiattarella, et al., 2011), there is no evidence of recent activity on the Alburni fault.

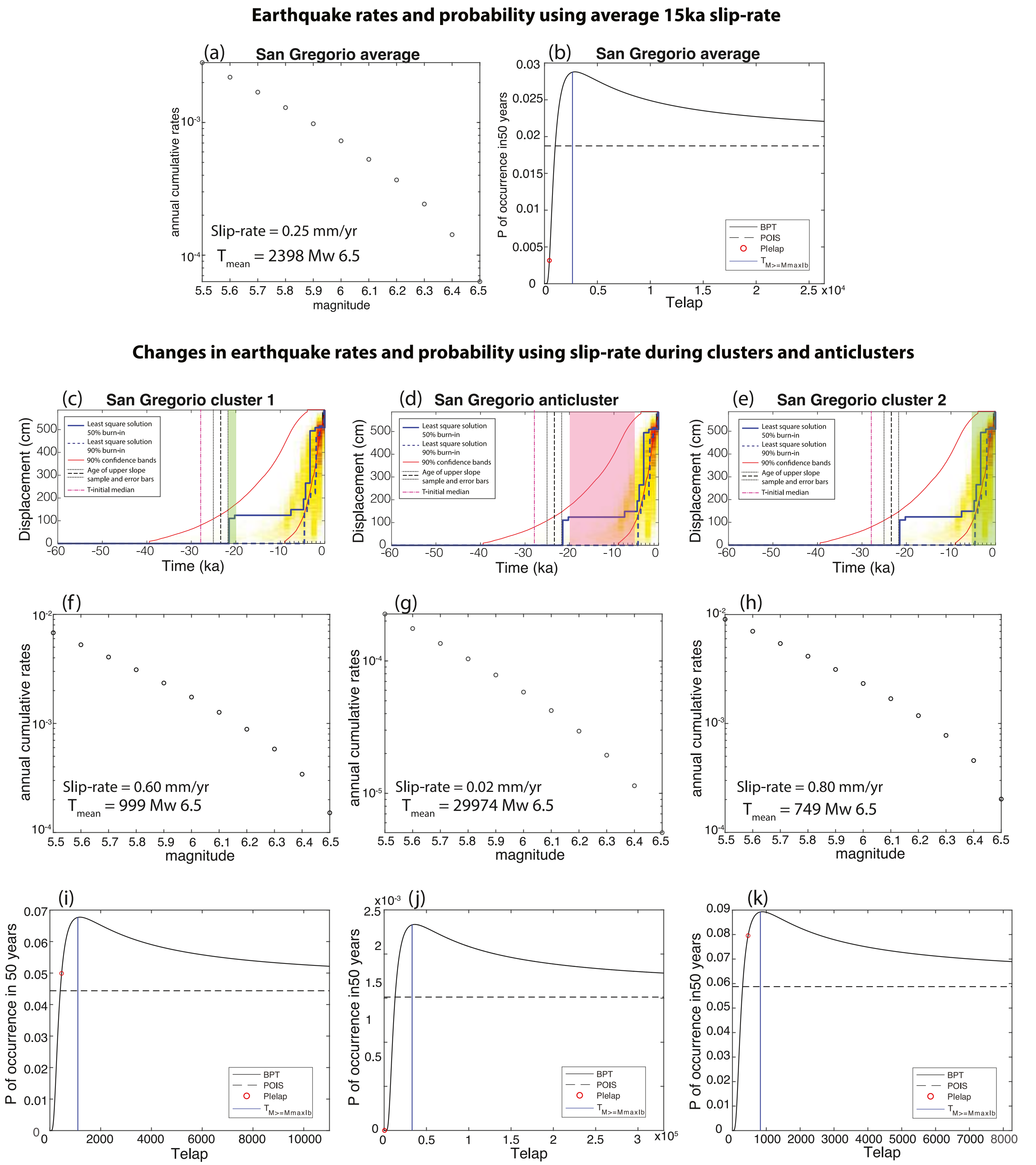

Figure 5. Implications of ^{36}Cl results on earthquake probability. (a)–(c) Times of clusters and anticlusters occurring on the San Gregorio Magno fault, based on interpretation of modeled slip histories. Green rectangles in panel (c) and (e) indicate the time of increased slip-rate; pink rectangle in panel (b) indicates the period of low slip-rate. (f)–(h) Cumulative annual rate of earthquakes with $5.5 \leq Mw \leq 6.6$ obtained with FiSH software (Pace et al., 2016). (i)–(k) Probability of occurrence of an earthquake with M_{max} 6.5 on the San Gregorio Magno fault during periods of clusters (I, k) and anticluster (j) calculated with FiSH software (Pace et al., 2016). Recurrence-time models shown are the Brownian passage time (BPT) model (black curve), the Poisson model (dashed line), and the time-dependent probability P\elap (red circle). The BPT and P\elap models are calculated for the next 50 years. The Poisson model refers to a 50-year period. The mean recurrence time of a magnitude that is equal or greater than the M_{max} 6.5 is also shown (vertical blue line).

Data Availability Statement

All data generated during this study are included in the Supplementary Information (https://doi.org/10.5281/zenodo.13255339, Sgambato et al., 2024). The code to model fault slip history from ^{36}Cl concentrations is published by Beck et al. (2018) (https://doi.org/10.5194/gmd-11-4383-2018). The exposure ages of the upper slope samples were obtained using the CRONUS online calculator published by Marrero et al. (2016) (https://doi.org/10.1016/j.quageo.2015.09.005).

Acknowledgments
This work was supported by a NERC Cosmogenic Isotope Analysis Facility Grant 9198/1019 (PI Gerald Roberts), and a NERC studentship (Grant NE/L002485/1) to Claudia Sgambato. We thank Dario Gioia and an anonymous reviewer for their help and constructive comments on our manuscript.

References

Aiello, G., Ascione, A., Barra, D., Munno, R., Petrosino, P., Ermolli, E. R., & Villani, F. (2007). Evolution of the late Quaternary San Gregorio Magno tectono-karstic basin (southern Italy) inferred from geomorphological, tephrostratigraphical and palaeoecological analyses: Tectonic implications. *Journal of Quaternary Science*, *22*(3), 233–245. https://doi.org/10.1002/jqs.1040

Allen, J. R., & Huntley, B. (2009). Last Interglacial palaeovegetation, palaeoenvironments and chronology: A new record from Lago Grande di Monticchio, southern Italy. *Quaternary Science Reviews*, *28*(15–16), 1521–1538. https://doi.org/10.1016/j.quascirev.2009.02.013

Amato, A., Aucelli, P. P. C., & Cinque, A. (2003). The long-term denudation rate in the Southern Apennines Chain (Italy): A GIS-aided estimation of the rock volumes eroded since middle Pleistocene time. *Quaternary International*, *101*, 3–11. https://doi.org/10.1016/S1040-6182(02)00087-3

Amicucci, L., Barchi, M. R., Montone, P., & Rubiliani, N. (2008). The Vallo di Diano and Auletta extensional basins in the southern Apennines (Italy): A simple model for a complex setting. *Terra Nova*, *20*(6), 475–482. https://doi.org/10.1111/j.1365-3121.2008.00841.x

Ascione, A., Caiazzo, C., & Cinque, A. (2007). Recent faulting in Southern Apennines (Italy); geomorphic evidence, spatial distribution and implications for rates of activity. *Bollettino della Societa Geologica Italiana*, *126*(2), 293–305.

Ascione, A., Cinque, A., Improta, L., & Villani, F. (2003). Late Quaternary faulting within the Southern Apennines seismic belt: New data from Mt. Marzano area (Southern Italy). *Quaternary International*, *101*, 27–41. https://doi.org/10.1016/s1040-6182(02)00127-1

Beck, J., Wolfers, S., & Roberts, G. P. (2018). Bayesian earthquake dating and seismic hazard assessment using chlorine-36 measurements (BED v1). *Geoscientific Model Development*, *11*(11), 4383–4397. https://doi.org/10.5194/gmd-11-4383-2018

Bello, S., Lavecchia, G., Andrenacci, C., Ercoli, M., Cirillo, D., Carboni, F., et al. (2022). Complex trans-ridge normal faults controlling large earthquakes. *Scientific Reports*, *12*(1), 10676. https://doi.org/10.1038/s41598-022-14406-4

Benedetti, L., Finkel, R., King, G., Armijo, R., Papanastassiou, D., Ryerson, F. J., et al. (2003). Motion on the Kaparelli fault (Greece) prior to the 1981 earthquake sequence determined from 36Cl cosmogenic dating. *Terra Nova*, *15*(2), 118–124. https://doi.org/10.1046/j.1365-3121.2003.00474.x

Benedetti, L., Finkel, R., Papanastassiou, D., King, G., Armijo, R., Ryerson, F., et al. (2002). Post-glacial slip history of the Sparta fault (Greece) determined by 36Cl cosmogenic dating: Evidence for non-periodic earthquakes. *Geophysical Research Letters*, *29*(8). https://doi.org/10.1029/2001GL014510

Benedetti, L., Manighetti, I., Gaudemer, Y., Finkel, R., Malavieille, J., Pou, K., et al. (2013). Earthquake synchrony and clustering on Fucino faults (Central Italy) as revealed from in situ 36Cl exposure dating. *Journal of Geophysical Research: Solid Earth*, *118*(9), 4948–4974. https://doi.org/10.1002/jgrb.50299

Benedetti, L., Tapponnier, P., King, G. C. P., & Piccardi, L. (1998). Surface rupture of the 1857 southern Italian earthquake? *Terra Nova*, *10*(4), 206–210. https://doi.org/10.1046/j.1365-3121.1998.00189.x

Blumetti, A. M., Grützner, C., Guerrieri, L., & Livio, F. (2017). Quaternary earthquakes: Geology and palaeoseismology for seismic hazard assessment. *Quaternary International*, *451*, 1–10. https://doi.org/10.1016/j.quaint.2017.04.002

Bollettinari, G., & Panizza, M. (1981). Una "Faglia di superficie" presso san Gregorio Magno in occasione del sisma del 23-XI-1980 in Irpinia.

Brozzetti, F. (2011). The Campania-Lucania Extensional Fault System, southern Italy: A suggestion for a uniform model of active extension in the Italian Apennines. *Tectonics*, *30*(5), TC5009. https://doi.org/10.1029/2010TC002794

Cavinato, G. P., & De Celles, P. G. (1999). Extensional basins in the tectonically bimodal central Apennines fold-thrust belt, Italy: Response to corner flow above a subducting slab in retrograde motion. *Geology*, *27*(10), 955–958. https://doi.org/10.1130/0091-7613(1999)027<0955:EBITTB>2.3.CO;2

Cello, G., Tondi, E., Micarelli, L., & Mattioni, L. (2003). Active tectonics and earthquake sources in the epicentral area of the 1857 Basilicata earthquake (southern Italy). *Journal of Geodynamics*, *36*(1–2), 37–50. https://doi.org/10.1016/S0264-3707(03)00037-1

Chiocci, F. L., Guerrieri, L., Monegato, G., & Pieruccini, P. (2023). Quaternary Map of Italy at the scale 1: 500,000. METIQ, ISPRA-SNPA, CNR, INGV, OGS, AISQ. Draft version for XXI INQUA.

Cowie, P., Phillips, R., Roberts, G., McCaffrey, K., Zijerveld, L. J. J., Gregory, L. C., et al. (2017). Orogen-scale uplift in the central Italian Apennines drives episodic behaviour of earthquake faults. *Scientific Reports*, *7*(1), 44858. https://doi.org/10.1038/srep44858

D'Addezio, G., Pantosti, D., & Valensise, G. (1991). Paleoearthquakes along the Irpinia fault at Pantano di San Gregorio Magno (southern Italy). *Il Quaternario*, *4*(1a), 121–136.

D'agostino, N., Giuliani, R., Mattone, M., & Bonci, L. (2001). Active crustal extension in the central Apennines (Italy) inferred from GPS measurements in the interval 1994–1999. *Geophysical Research Letters*, *28*(10), 2121–2124. https://doi.org/10.1029/2000GL012462

Devoti, R., Pietrantonio, G., & Riguzzi, F. (2014). GNSS networks for geodynamics in Italy. *Física de la Tierra*, *26*(0), 11–24. https://doi.org/10.5209/rev_fite.2014.v26.46968

Dolan, J. F., Bowman, D. D., & Sammis, C. G. (2007). Long-range and long-term fault interactions in Southern California. *Geology*, *35*(9), 855–858. https://doi.org/10.1130/G23789A.1

Dolan, J. F., McAuliffe, L. J., Rhodes, E. J., McGill, S. F., & Zinke, R. (2016). Extreme multi-millennial slip rate variations on the Garlock fault, California: Strain super-cycles, potentially time-variable fault strength, and implications for system-level earthquake occurrence. *Earth and Planetary Science Letters*, *446*, 123–136. ISSN 0012-821X. https://doi.org/10.1016/j.epsl.2016.04.011

Dolan, J. F., Van Dissen, R. J., Rhodes, E. J., Zinke, R., Hatem, A. E., McGuire, C., et al. (2024). One tune, many tempos: Faults trade off slip in time and space to accommodate relative plate motions. *Earth and Planetary Science Letters*, *625*, 118484. https://doi.org/10.1016/j.epsl.2023.118484

Dunai, T. J. (2010). *Cosmogenic nuclides: Principles, concepts and applications in the earth surface sciences*. Cambridge University Press.

Faure Walker, J. P., Roberts, G. P., Cowie, P. A., Papanikolaou, I., Michetti, A. M., Sammonds, P., et al. (2012). Relationship between topography, rates of extension and mantle dynamics in the actively-extending Italian Apennines. *Earth and Planetary Science Letters*, *325*, 76–84. https://doi.org/10.1016/j.epsl.2012.01.028

Galli, P., Bosi, V., Piscitelli, S., Giocoli, A., & Scionti, V. (2006). Late Holocene earthquakes in southern Apennine: Paleoseismology of the Caggiano fault. *International Journal of Earth Sciences*, *95*(5), 855–870. https://doi.org/10.1007/s00531-005-0066-2

Galli, P., & Galadini, F. (2003). Disruptive earthquakes revealed by faulted archaeological relics in Samnium (Molise, southern Italy). *Geophysical Research Letters*, *30*(5), 1266. https://doi.org/10.1029/2002GL016456

Galli, P., & Peronace, E. (2014). New paleoseismic data from the Irpinia Fault. A different seismogenic perspective for southern Apennines (Italy). *Earth-Science Reviews*, *136*, 175–201. https://doi.org/10.1016/j.earscirev.2014.05.013

Gelman, A., & Rubin, D. B. (1992). Inference from iterative simulation using multiple sequences. *Statistical Science*, *7*(4), 457–472. https://doi.org/10.1214/ss/1177011136

Giano, S. I., Gioia, D., & Schiattarella, M. (2014). Morphotectonic evolution of connected intermontane basins from the southern Apennines, Italy: The legacy of the pre-existing structurally controlled landscape. *Rendiconti Lincei*, *25*(S2), 241–252. https://doi.org/10.1007/s12210-014-0325-x

Gioia, D., Martino, C., & Schiattarella, M. (2011). Long-to short-term denudation rates in the southern Apennines: Geomorphological markers and chronological constraints. *Geologica Carpathica*, *62*(1), 27–41. https://doi.org/10.2478/v10096-011-0003-1

Gioia, D., Schiattarella, M., Mattei, M., & Nico, G. (2011). Quantitative morphotectonics of the Pliocene to Quaternary Auletta basin, southern Italy. *Geomorphology*, *134*(3–4), 326–343. https://doi.org/10.1016/j.geomorph.2011.07.009

Giraudi, C., & Frezzotti, M. (1997). Late Pleistocene glacial events in the central Apennines, Italy. *Quaternary Research*, *48*(3), 280–290. https://doi.org/10.1006/qres.1997.1928

Goodall, H. J., Gregory, L. C., Wedmore, L. N. J., McCaffrey, K. J. W., Amey, R. M. J., Roberts, G. P., et al. (2021). Determining histories of slip on normal faults with bedrock scarps using cosmogenic nuclide exposure data. *Tectonics*, *40*(3), e2020TC006457. https://doi.org/10.1029/2020TC006457

Guidoboni, E., Ferrari, G., Mariotti, D., Comastri, A., Tarabusi, G., Sgattoni, G., & Valensise, G. (2018). *CFTI5Med, Catalogo dei Forti Terremoti in Italia (461 a.C.-1997) e nell'area Mediterranea (760 a.C.-1500)*. Istituto Nazionale di Geofisica e Vulcanologia (INGV). https://doi.org/10.6092/ingv.it-cfti5

Guidoboni, E., Ferrari, G., Tarabusi, G., Sgattoni, G., Comastri, A., Mariotti, D., et al. (2019). CFTI5Med, the new release of the catalogue of strong earthquakes in Italy and in the Mediterranean area. *Scientific Data*, *6*(1), 80. https://doi.org/10.1038/s41597-019-0091-9

Iezzi, F., Francescone, M., Pizzi, A., Blumetti, A., Boncio, P., Di Manna, P., et al. (2023). Slip localization on multiple fault splays accommodating distributed deformation across normal fault complexities. *Tectonophysics*, *868*, 230075. https://doi.org/10.1016/j.tecto.2023.230075

Iezzi, F., Roberts, G., Faure Walker, J., Papanikolaou, I., Ganas, A., Deligiannakis, G., et al. (2021). Temporal and spatial earthquake clustering revealed through comparison of millennial strain-rates from 36Cl cosmogenic exposure dating and decadal GPS strain-rate. *Scientific Reports*, *11*(1), 23320. https://doi.org/10.1038/s41598-021-02131-3

Kagan, Y. Y., & Jackson, D. D. (1991). Long-term earthquake clustering. *Geophysical Journal International*, *104*(1), 117–133. https://doi.org/10.1111/j.1365-246X.1991.tb02498.x

King, G. C., Stein, R. S., & Lin, J. (1994). Static stress changes and the triggering of earthquakes. *Bulletin of the Seismological Society of America*, *84*(3), 935–953. https://doi.org/10.1785/BSSA0840030935

Marrero, S. M., Phillips, F. M., Borchers, B., Lifton, N., Aumer, R., & Balco, G. (2016). Cosmogenic nuclide systematics and the CRONUScalc program. *Quaternary Geochronology*, *31*, 160–187. https://doi.org/10.1016/j.quageo.2015.09.005

Mechernich, S., Reicherter, K., Deligiannakis, G., & Papanikolaou, I. (2023). Tectonic geomorphology of active faults in Eastern Crete (Greece) with slip rates and earthquake history from cosmogenic 36Cl dating of the Lastros and Orno faults. *Quaternary International*, *651*, 77–91. https://doi.org/10.1016/j.quaint.2022.04.007

Mechernich, S., Schneiderwind, S., Mason, J., Papanikolaou, I. D., Deligiannakis, G., Pallikarakis, A., et al. (2018). The seismic history of the Pisia fault (eastern Corinth rift, Greece) from fault plane weathering features and cosmogenic 36Cl dating. *Journal of Geophysical Research: Solid Earth*, *123*(5), 4266–4284. https://doi.org/10.1029/2017JB014600

Mildon, Z. K., Roberts, G. P., Faure Walker, J. P., Beck, J., Papanikolaou, I., Michetti, A. M., et al. (2022). Surface faulting earthquake clustering controlled by fault and shear-zone interactions. *Nature Communications*, *13*(1), 7126. https://doi.org/10.1038/s41467-022-34821-5

Moore, J. D., & Parsons, B. (2015). Scaling of viscous shear zones with depth-dependent viscosity and power-law stress–strain-rate dependence. *Geophysical Journal International*, *202*(1), 242–260. https://doi.org/10.1093/gji/ggv143

Mozafari, N., Özkaymak, Ç., Tikhomirov, D., Ivy-Ochs, S., Alfimov, V., Sözbilir, H., et al. (2021). Seismic activity of the Manisa Fault Zone in Western Turkey constrained by cosmogenic 36Cl dating. *Geosciences*, *11*(11), 451. https://doi.org/10.3390/geosciences11110451

Mozafari, N., Tikhomirov, D., Sumer, Ö., Özkaymak, Ç., Uzel, B., Yeşilyurt, S., et al. (2019). Dating of active normal fault scarps in the Büyük Menderes Graben (western Anatolia) and its implications for seismic history. *Quaternary Science Reviews*, *220*, 111–123. https://doi.org/10.1016/j.quascirev.2019.07.002

Nicol, A., Walsh, J., Berryman, K., & Villamor, P. (2006). Interdependence of fault displacement rates and paleoearthquakes in an active rift. *Geology*, *34*(10), 865–868. https://doi.org/10.1130/G22335.1

Pace, B., Visini, F., & Peruzza, L. (2016). FiSH: MATLAB tools to turn fault data into seismic-hazard models. *Seismological Research Letters*, *87*(2A), 374–386. https://doi.org/10.1785/0220150189

Palumbo, L., Benedetti, L., Bourlès, D., Cinque, A., & Finkel, R. (2004). Slip history of the Magnola fault (Apennines, Central Italy) from 36Cl surface exposure dating: Evidence for strong earthquakes over the Holocene. *Earth and Planetary Science Letters*, *225*(1–2), 163–176. https://doi.org/10.1016/j.epsl.2004.06.012

Pantosti, D., D'Addezio, G., & Cinti, F. R. (1993). Paleoseismological evidence of repeated large earthquakes along the 1980 Irpinia earthquake fault. *Annali di Geofisica*, *36*(1), 321–330. https://doi.org/10.4401/ag-4317

Pantosti, D., Schwartz, D. P., & Valensise, G. (1993). Paleoseismology along the 1980 surface rupture of the Irpinia Fault: Implications for earthquake recurrence in the southern Apennines, Italy. *Journal of Geophysical Research*, *98*(B4), 6561–6577. https://doi.org/10.1029/92JB02277

Pantosti, D., & Valensise, G. (1990). Faulting mechanism and complexity of the November 23, 1980, Campania-Lucania Earthquake, inferred from surface observations. *Journal of Geophysical Research*, *95*(B10), 15319–15341. https://doi.org/10.1029/JB095iB10p15319

Papanikolaou, I. D., & Roberts, G. P. (2007). Geometry, kinematics and deformation rates along the active normal fault system in the southern Apennines: Implications for fault growth. *Journal of Structural Geology*, *29*(1), 166–188. https://doi.org/10.1016/j.jsg.2006.07.009

Piccardi, L., Gaudemer, Y., Tapponnier, P., & Boccaletti, M. (1999). Active oblique extension in the central Apennines (Italy): Evidence from the Fucino region. *Geophysical Journal International*, *139*(2), 499–530. https://doi.org/10.1046/j.1365-246x.1999.00955.x

Roberts, G. P., & Michetti, A. M. (2004). Spatial and temporal variations in growth rates along active normal fault systems: An example from The Lazio–Abruzzo Apennines, central Italy. *Journal of Structural Geology*, *26*(2), 339–376. https://doi.org/10.1016/S0191-8141(03)00103-2

Roberts, G. P., Sgambato, C., Mildon, Z. K., Iezzi, F., Beck, J., Robertson, J., et al. (2024). Spatial migration of temporal earthquake clusters driven by the transfer of differential stress between neighbouring fault/shear-zone structures. *Journal of Structural Geology*, *181*, 105096. https://doi.org/10.1016/j.jsg.2024.105096

Rovida, A., Locati, M., Camassi, R., Lolli, B., & Gasperini, P. (2020). The Italian earthquake catalogue CPTI15. *Bulletin of Earthquake Engineering*, *18*(7), 2953–2984. https://doi.org/10.1007/s10518-020-00818-y

Rovida, A., Locati, M., Camassi, R., Lolli, B., Gasperini, P., & Antonucci, A. (2022). Italian parametric earthquake catalogue (CPTI15) version 4.0 [Dataset]. Istituto Nazionale di Geofisica e Vulcanologia (INGV). https://doi.org/10.13127/cpti/cpti15.4

Schiattarella, M., Beneduce, P., Capolongo, D., Di Leo, P., Giano, S. I., Gioia, D., et al. (2008). Uplift and erosion rates from the southern Apennines, Italy. *Bollettino di Geofisica Teorica ed Applicata*, *49*(2), 470–475.

Schlagenhauf, A., Gaudemer, Y., Benedetti, L., Manighetti, I., Palumbo, L., Schimmelpfennig, I., et al. (2010). Using in situ Chlorine-36 cosmonuclide to recover past earthquake histories on limestone normal fault scarps: A reappraisal of methodology and interpretations. *Geophysical Journal International*, *182*(1), 36–72. https://doi.org/10.1111/j.1365-246X.2010.04622.x

Schlagenhauf, A., Manighetti, I., Benedetti, L., Gaudemer, Y., Finkel, R., Malavieille, J., & Pou, K. (2011). Earthquake supercycles in Central Italy, inferred from 36Cl exposure dating. *Earth and Planetary Science Letters*, *307*(3–4), 487–500. https://doi.org/10.1016/j.epsl.2011.05.022

Serpelloni, E., Anzidei, M., Baldi, P., Casula, G., & Galvani, A. (2005). Crustal velocity and strain-rate fields in Italy and surrounding regions: New results from the analysis of permanent and non-permanent GPS networks. *Geophysical Journal International*, *161*(3), 861–880. https://doi.org/10.1111/j.1365-246X.2005.02618.x

Serpelloni, E., Cavaliere, A., Martelli, L., Pintori, F., Anderlini, L., Borghi, A., et al. (2022). Surface velocities and strain-rates in the Euro-Mediterranean region from massive GPS data processing. *Frontiers in Earth Science*, *10*, 907897. https://doi.org/10.3389/feart.2022.907897

Sgambato, C., Faure Walker, J. P., Mildon, Z. K., & Roberts, G. P. (2020). Stress loading history of earthquake faults influenced by fault/shear zone geometry and Coulomb pre-stress. *Scientific Reports*, *10*(1), 12724. https://doi.org/10.1038/s41598-020-69681-w

Sgambato, C., Faure Walker, J. P., Roberts, G. P., Mildon, Z. K., & Meschis, M. (2023). Influence of fault system geometry and slip rates on the relative role of coseismic and interseismic stresses on earthquake triggering and recurrence variability. *Journal of Geophysical Research: Solid Earth*, *128*(11), e2023JB026496. https://doi.org/10.1029/2023JB026496

Sgambato, C., Roberts, G., Iezzi, F., Faure Walker, J., Beck, J., Mildon, Z., et al. (2024). Millennial slip-rates variability of along-strike active faults in the Italian Southern Apennines revealed by cosmogenic 36Cl dating of fault scarps [Dataset]. *Zenodo*. https://doi.org/10.5281/zenodo.13255340

Sgambato, C., Walker, J. P. F., & Roberts, G. P. (2020). Uncertainty in strain-rate from field measurements of the geometry, rates and kinematics of active normal faults: Implications for seismic hazard assessment. *Journal of Structural Geology*, *131*, 103934. https://doi.org/10.1016/j.jsg.2019.103934

Sieh, K., Stuiver, M., & Brillinger, D. (1989). A more precise chronology of earthquakes produced by the San Andreas Fault in southern California. *Journal of Geophysical Research*, *94*(B1), 603–623. https://doi.org/10.1029/JB094iB01p00603

Soliva, R., Benedicto, A., Schultz, R. A., Maerten, L., & Micarelli, L. (2008). Displacement and interaction of normal fault segments branched at depth: Implications for fault growth and potential earthquake rupture size. *Journal of Structural Geology*, *30*(10), 1288–1299. https://doi.org/10.1016/j.jsg.2008.07.005

Stein, R. S., Barka, A. A., & Dieterich, J. H. (1997). Progressive failure on the North Anatolian fault since 1939 by earthquake stress triggering. *Geophysical Journal International*, *128*(3), 594–604. https://doi.org/10.1111/j.1365-246X.1997.tb05321.x

Stone, J. O. (2000). Air pressure and cosmogenic isotope production. *Journal of Geophysical Research*, *105*(B10), 23753–23759. https://doi.org/10.1029/2000JB900181

Stone, J. O., Allan, G. L., Fifield, L. K., & Cresswell, R. G. (1996). Cosmogenic chlorine-36 from calcium spallation. *Geochimica et Cosmochimica Acta*, *60*(4), 679–692. https://doi.org/10.1016/0016-7037(95)00429-7

Tesson, J., & Benedetti, L. (2019). Seismic history from in situ 36Cl cosmogenic nuclide data on limestone fault scarps using Bayesian reversible jump Markov chain Monte Carlo. *Quaternary Geochronology*, *52*, 1–20. https://doi.org/10.1016/j.quageo.2019.02.004

Tikhomirov, D., Amiri, N. M., Ivy-Ochs, S., Alfimov, V., Vockenhuber, C., & Akçar, N. (2019). Fault Scarp Dating Tool-a MATLAB code for fault scarp dating using in-situ chlorine-36 supplemented with datasets of Yavansu and Kalafat faults. *Data in Brief*, *26*, 104476. https://doi.org/10.1016/j.dib.2019.104476

Tucker, G. E., McCoy, S. W., Whittaker, A. C., Roberts, G. P., Lancaster, S. T., & Phillips, R. (2011). Geomorphic significance of postglacial bedrock scarps on normal-fault footwalls. *Journal of Geophysical Research*, *116*(F1). https://doi.org/10.1029/2010JF001861

Villani, F., & Pierdominici, S. (2010). Late Quaternary tectonics of the Vallo di Diano basin (southern Apennines, Italy). *Quaternary Science Reviews*, *29*(23–24), 3167–3183. https://doi.org/10.1016/j.quascirev.2010.07.003

Wells, D. L., & Coppersmith, K. J. (1994). New empirical relationships among magnitude, rupture length, rupture width, rupture area, and surface displacement. *Bulletin of the Seismological Society of America*, *84*(4), 974–1002. https://doi.org/10.1785/BSSA0840040974

Westaway, R., & Jackson, J. (1987). The earthquake of 1980 November 23 in Campania—Basilicata (southern Italy). *Geophysical Journal International*, *90*(2), 375–443. https://doi.org/10.1111/j.1365-246X.1987.tb00733.x

Zerathe, S., Lebourg, T., Braucher, R., & Bourlès, D. (2014). Mid-Holocene cluster of large-scale landslides revealed in the Southwestern Alps by ^{36}Cl dating. Insight on an Alpine-scale landslide activity. *Quaternary Science Reviews*, *90*, 106–127. https://doi.org/10.1016/j.quascirev.2014.02.015